

ARTICLE

## Conception the Fluid Flow Behavior within Oil Reservoir Rock by Using Computed Tomography (CT) Scan

Amani J. Majeed<sup>1\*</sup> Falah A Abood<sup>2</sup> Ahmed K. Alshara<sup>3</sup>

1. Petroleum Engineering Department, University of Basrah, Iraq

2. Mechanical Engineering Department, University of Basrah, Iraq

3. Mechanical Engineering Department, University of Misan, Iraq

---

ARTICLE INFO

*Article history*

Received: 3 May 2021

Accepted: 2 June 2021

Published Online: 25 August 2021

---

*Keywords:*

Computed Tomography (CT) scan

Al-Nour field

Fluid flow

---

ABSTRACT

The behavior of fluid flow has been studied during the different flow media over the past decades. In addition, the behavior of the flow of fluid through porous media has garnered much research interest. This paper sheds light on fissured rocks of oil reservoir media (as one of the porous media domain), and the effect of these fissured on fluid flow. In this article, the Finite Volume Method (FVM) has been used to visualize the behavior of single-phase fluid flow in an actual core according to the dual-porosity dual permeability model. The study was conducted in two parts, the first was the image processing for one of the real oil reservoir fractured rock images, where the image was processed and simulated by ANSYS-CFX software, and the results showed a complete visualizing of the fluid behavior during this domain. As for the other side, a simulation of a real reservoir rock belonging to the Al-Nour field in Iraq / Misan was made. The X-ray Computed Tomography (CT) scan has been used to convert the real fractured core to a dynamic domain. ANSYS-CFX program has been used and the results illustrated the pressure counter, the velocity counter, the velocity streamline, and the velocity vectors for the studied model in three dimensions. A comparison was made between the productivity index for fractured and non-fractured rock and the results explained that the presence of fracture can improve the productivity index to about 5.74%.

### 1. Introduction

Natural fractures are found in almost all petroleum reservoirs. These structures are difficult in their characterization and predictor. Representing the fluid flow behavior in a naturally fractured reservoir is very complex because of the complex nature of these domains. This topic took the attention of both engineers and geologists [1-3]. Two media could be recognized in this type of reservoir; fracture media and matrix media. The fracture

and matrix are different in their porosity and permeability. The effect of the fracture and fracture permeability on the flow of fluid has been notarized by many studies, where these fissures may act as a barriers system, conduits system, or combined (conduit-barrier) systems [4,5]. A comprehensive study of the effect of fractures on the fluid flow within the subsurface has been given by scientists [6-12]. In 1990, Luthi and Souhait, performed 3D finite element models to investigate the response to fissures of the Formation Micro-Scanner, where a high resolution

---

*\*Corresponding Author:*

*Amani J. Majeed*

*Petroleum Engineering Department, University of Basrah, Iraq;*

*Email: [Amani.majeed@uobasrah.edu.iq](mailto:Amani.majeed@uobasrah.edu.iq)*

has been recorded for electrical scans for the borehole wall according to fissures. The detected, traced, and quantified fissures were the 3-steps that they used in their model. In the detection step, they used the Formation Micro-Scanner images for the locations that possibly had fissures, so when the electric conductivity overrides the local conductivity of the matrix by a statistically considerable amount the fracture locations are detected. After that, they performed an integration around these locations over a circular zone to gather all excessive currents; then the integral reduced to approximate the line integral. The trace step has been done by a line sharpening and neighbor connectivity tests then the apertures are computed for whole fissure locations. From the obtained results, they showed that their method successfully traces fractures, and their technique was novel and unique for characterizing fissures in wellbores<sup>[13]</sup>. In 2003, Hirono et. al, used the n X-ray computed tomography (CT) imaging method to visualize the behavior of fluid during the permeability testing. Moreover, along the permeable zone, they measured the localized permeabilities<sup>[14]</sup>. In 2007, Karpyn et. al., studied the fissures' effect on the two-phase flow of fluid (oil and water), and they used micro-

computed tomography (MCT) to distinguish the internal structure of the fracture.

The focus of this research was on visualizing the flow inside the fractures differently, as several programs were used to obtain a comprehensive visualization of a single-phase fluid flow in these media. Moreover, the X-ray Computed Tomography (CT) scan has been used to convert the real fractured core (the core that was taken from the Al-Nour field in Iraq / Misan) to a dynamic domain, where several programs have been used to get a three-dimensional dynamic domain for the mentioned core.

## 2. Methodology

The behavior of fluid flow through a fracture profile in a permeable rock in an actual reservoir core, shown in Figure 1, according to dual-porosity-dual-permeability (DPDP) model has been performed numerically in this study. The study falls into two domains; the first one represents the simulation of a natural fracture picture, as shown in Figure 2. While the second one represents the simulation of the real fractured core. Where, the X-ray

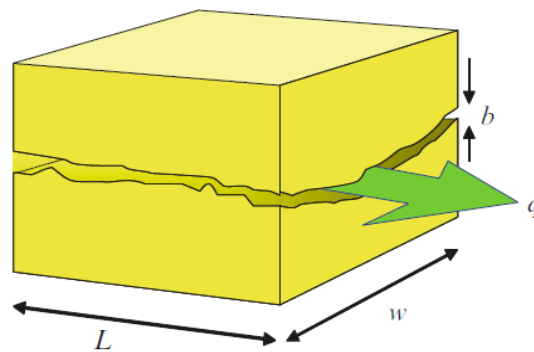


Figure 1. Flow in actual fracture



Figure 2. Fractures and Matrices.<sup>[16]</sup>

Computed Tomography (CT) scan was used to get a 3D picture of the real fractured core, as illustrated in Figure 3. This image was subjected to a series of software operations to be converted from a static model that can't be simulated, into a dynamic model that can be simulated. Figure 4 shows the chart for the series of programs used in image processing.

Two media could be recognized in this type of rock; fracture media and matrix media. The general form of mass balance equations can be given as [17,18];

- The mass balance equation for the fluid flow in the matrix system is given by the following equation

$$\frac{\partial \phi^m s^m}{\partial t} + \nabla \cdot \mathbf{u}^m = q^{f-m} + \psi^m \quad (1)$$

where the phase fluxes in matrix ( $\mathbf{u}^m$ ) is given by:

$$\mathbf{u}^m = - \frac{K_r^m K^m}{\mu} [\nabla P^m - \rho g] \quad (2)$$

- The mass balance equation for the fluid flow in the fracture system is given by the following equation:

$$\frac{\partial \phi^f s^f}{\partial t} + \nabla \cdot \mathbf{u}^f = q^{m-f} + \psi^f \quad (3)$$

where the phase fluxes in fracture ( $\mathbf{u}^f$ ) is given by:

$$\mathbf{u}^f = - \frac{K_r^f K^f}{\mu} [\nabla P^f - \rho g] \quad (4)$$

Where,  $\phi$  is the porosity,  $s$  is the phase saturation,  $q$  is the volumetric flux,  $\psi$  is the volumetric source,  $K_r$  is a

relative permeability, and the superscripts;  $f$  and  $m$  denote to the parameters which defined in fracture and matrix domains, respectively.

Moreover, the general form of a momentum conservation equation (Navier-Stokes equation) can be given as [19];

$$\rho \frac{D \mathbf{u}}{Dt} = - \nabla P - \mu \frac{\mathbf{u}}{k} + \mu_{eff} \nabla^2 \mathbf{u} \quad (5)$$

Where;

$$\mu \approx \mu_{eff} \quad \text{For large value of } k$$

Darcy introduced an equation for the mean filter velocity  $\mathbf{u}$  for the fluid flow through a homogeneous porous media field with absolute permeability  $k$ , a viscosity of the fluid  $\mu$ , and pressure gradient across the domain  $\nabla P$ :

$$\mathbf{u} = - \frac{k}{\mu} (\nabla P - \rho g) \quad (6)$$

where

$g$  = The acceleration due to the gravitational forces, which can be neglected for a horizontal layer flow ( $\text{ft/s}^2$ ).

$\rho$  = The density of the fluid ( $\text{lb/ft}^3$ ).

The mean filter velocity in Equation (3.7), is also called Darcy velocity, which is related to the average pore velocity  $\mathbf{u}_p$  by the relation [20];

$$\mathbf{u} = \phi \mathbf{u}_p \quad (7)$$

Where  $\phi$  is the effective porosity of the porous media.

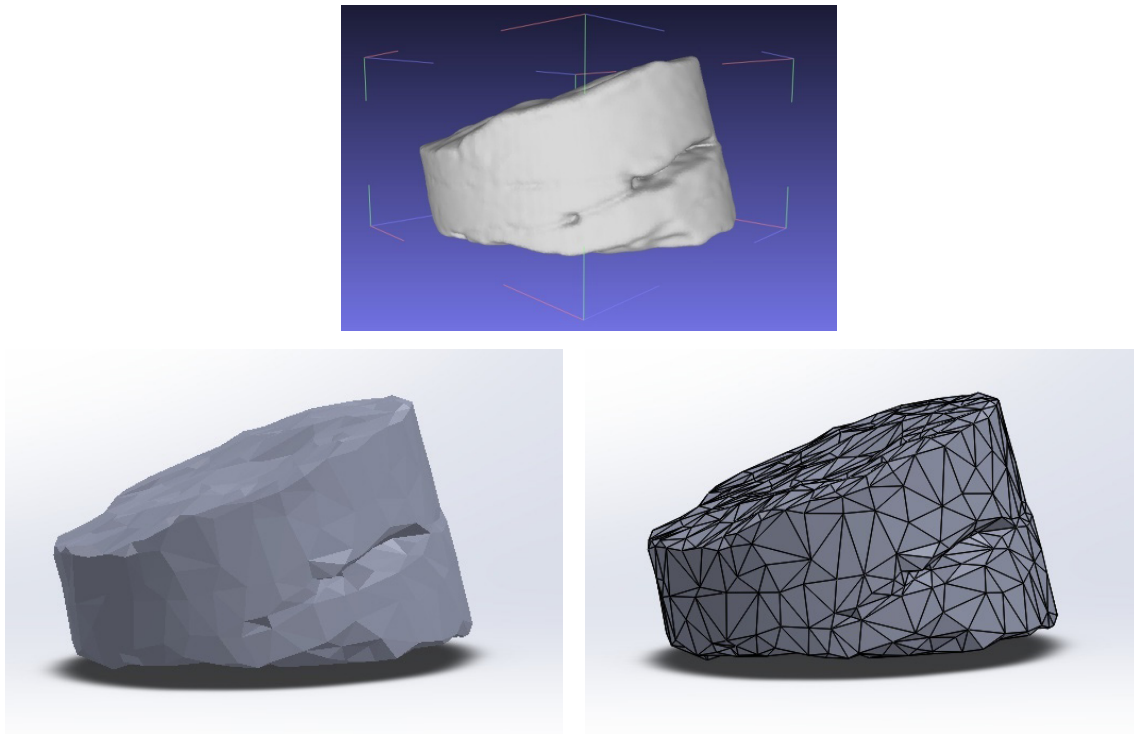


Figure 3. Actual Fractured core.

$$k_f = \frac{h_{avg}^2}{12} \quad (8)$$

Where  $h_{avg}$  is an average value for  $h_i$ , which can be calculated from the following:

$$h_{avg} = \frac{\sum_{i=1}^n h_i}{n} \quad (9)$$

For the single-phase flow conditions, the productivity index ( $J$ ) defined as the relationship between flow rate and the pressure drawdown, the difference between a given average reservoir pressure and the bottom-hole flowing pressure:

$$J = \frac{q_o}{\bar{P}_R - P_{wf}} \quad (10)$$

Where;  $q_o$  is the oil flow rate,  $\bar{P}_R$  the average reservoir pressure, and  $P_{wf}$  is the bottomhole pressure.

The parameters boundary conditions are; Fluid density = 49.94 lb/ft<sup>3</sup> (0.8 g/cm<sup>3</sup>), Fluid viscosity = 0.00010443 lbf s ft<sup>-2</sup> (5 cp), The total pressure inlet = 3000 psi (2.068E7 Pa), No-slip wall conditions, and homogenous domain have been assumed.

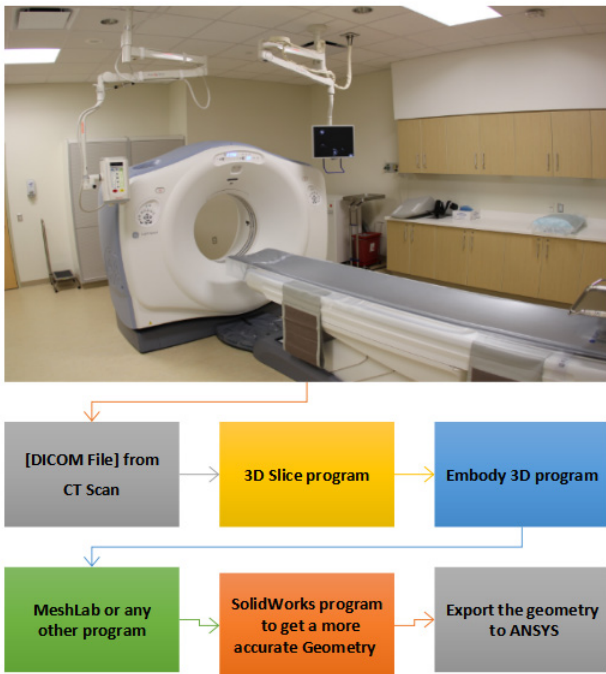


Figure 4. The CT-scan image transition.

### 3. Results and Discussion

The single-phase fluid flow is presupposed to be laminar and follow Darcy’s Law. Moreover, the EbFV approach has been used in the analysis and the results in detail have been explained. The X-ray Computed Tomography (CT) scan was used to convert the actual

rock domain to a dynamic picture domain, to make it suitable for simulating by the ANSYS-CFX program.

Figure 5-A represents the real image from which the measurements of the fracture were taken. While Figure 5-B represents the computational domain that corresponds to this image that was executed in the ANSYS program, CFX package. The average fracture apertures have been calculated in this model, where it is approximately (1.42 cm), which in turn can be used to calculate the permeability of fracture by using Equation 8.

Figure 6 shows the pressure contour throughout the computational domain where pressure gradient can be observed through the domain as a whole, in addition, to illustrate the pressure distribution through the fractured area.

Figure 7 illustrates the velocity contour throughout the computational domain. A rapid velocity increase in the fractured zone can be observed, which is attributed to its high permeability when compared to the permeability of the surrounding rock. Where the average velocity in the fracture is (0.007151 m/s, Re = 16.13), while the average velocity in the matrix is (0.00008143 m/s).

Figure 8 and Figure 9, visualize the velocity streamline and the velocity vectors throughout the computational domain, respectively, under (1000 psi) pressure drop and with fracture permeability equal to (0.0000168 m<sup>2</sup>). Where the velocity streamline can be followed throughout the domain to move from the areas of high pressure to low pressure, in addition to the distribution within the fractured zone. The incoming velocity vectors to the fractured zone have been enlarged to give further indication of intensified fluid movement in this area.

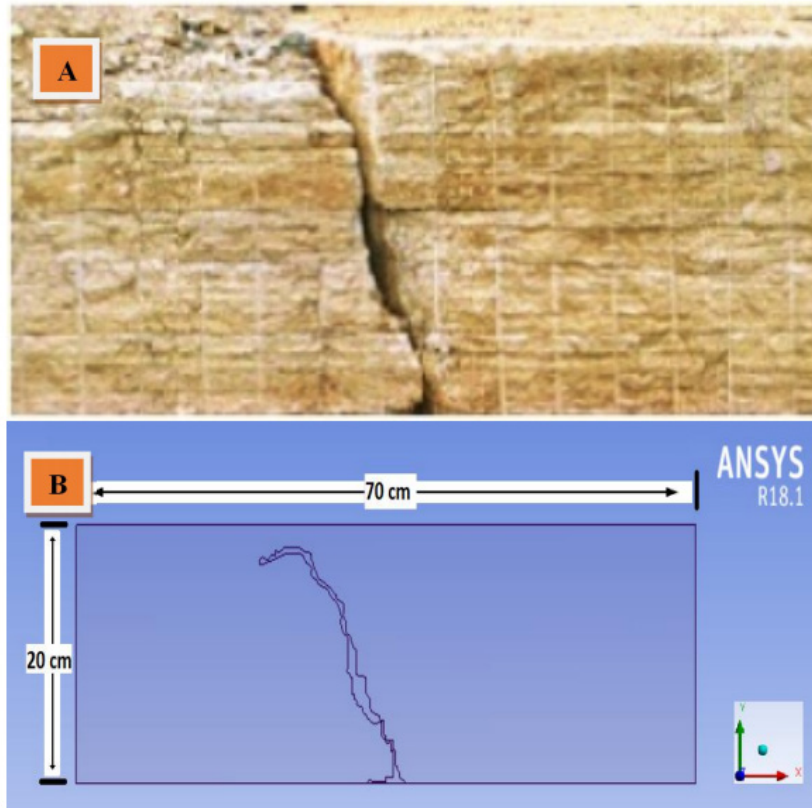
On the other hand, the simulation of a real rock model (with 10.5 cm in diameter and 5.5 cm in length) obtained from the Misan Field, Bin Umar formation, at a depth (3688 m) was done. The tomography scan has been taken to the rock by using a CT scan device belonging to Al-Fayhaa Hospital, where a total of CT scan pictures have been obtained and several programs were treated so that the geometry could be converted into a 3D dynamic domain that could be simulated by ANSYS. These processes would convert the geometrical form of a static model into a dynamic model that can be manipulated with engineering programs and undergone the boundary conditions that are related to a special issue, as shown in Figure 10. The average fracture aperture is about (1.9054 cm). Here also the Equation (8) could be used to calculate the permeability of the fracture.

Figure 11 displays the pressure contour and the velocity contour if it is presumed that the rock without any fracture. Where the pressure drop during the rock is 1000

psi, while the average velocity on the outlet approximately (0.0001538 m/s). The velocity streamlines and the velocity vectors of the fluid during the non-fractured rock are depicted in Figure 12.

The pressure contour and the velocity contour of fractured rock illustrate in Figure 13. Obviously, the

presence of a small fracture can contribute to raising the rate of fluid velocity where the average velocity of the outflow fluid reaches about (0.000162467 m/s). The difference in the pressure contour lines in both the fractured and non-cracked rock is illustrated in Figure 15, where the pressure lines are distributed clearly in



**Figure 5.** (A) Real fractured rock image, (B) The domain that has been designed by ANSYS program

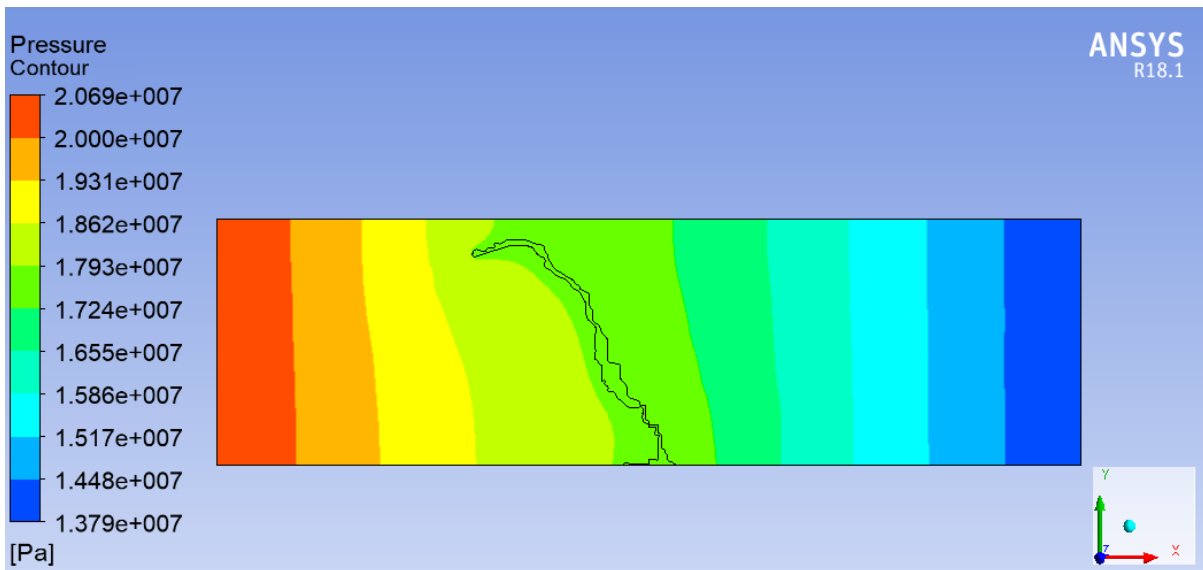


**Figure 6.** The Global pressure contour throughout the domain

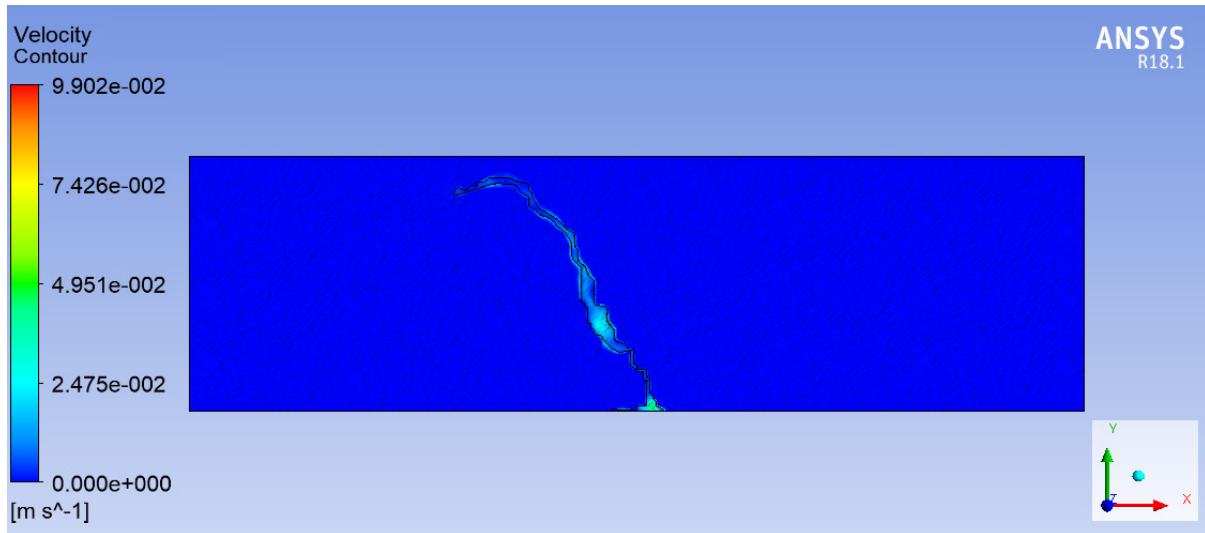


Figure 7. The velocity contour throughout the domain.

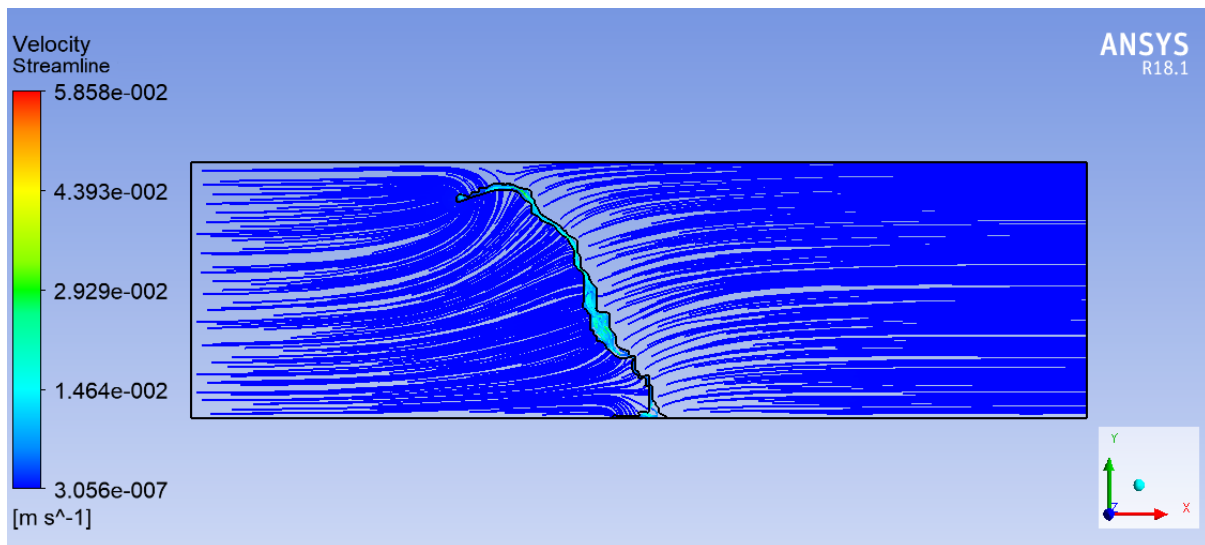


Figure 8. The velocity streamline throughout the domain.

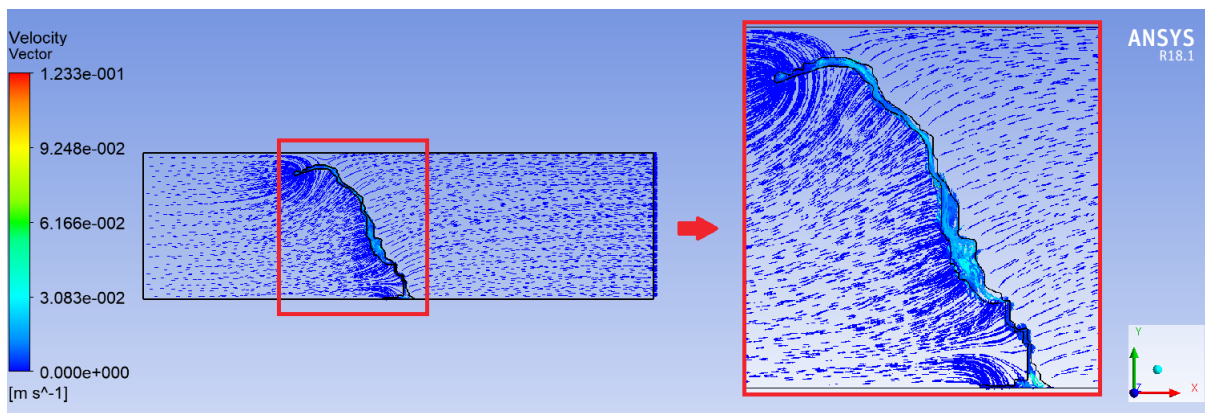
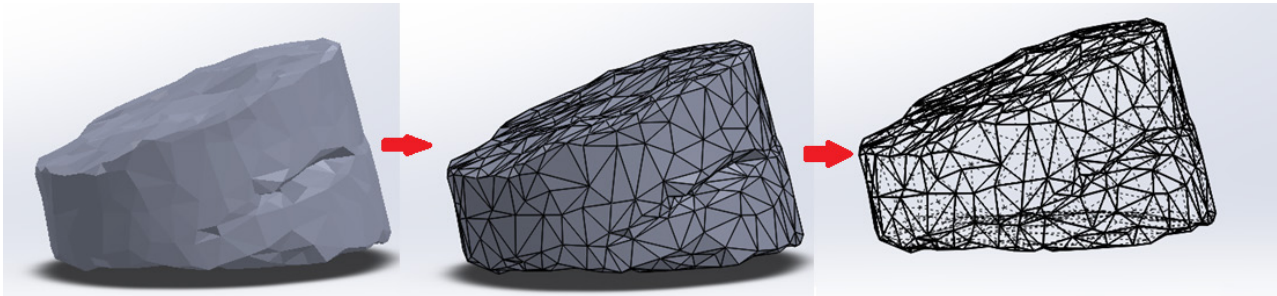


Figure 9. The velocity vectors throughout the domain.

both cases. In the absence of a fracture, the pressure distribution will be uniform to all layers of the rock from the high-pressure area to the low-pressure zone. In the case of fractured rock, the pressure will decrease at all sides of the fracture faster than adjacent layers. This is due to the high permeability of the fracture when compared with the matrix.

The velocity streamlines and the velocity vectors of

the fluid over the fractured rock are depicted in Figure 14, where an increase in fluid velocity can be observed in the fracture zone, this is a reasonable behavior as the fluid would be attracted to the areas with high permeability. A comparison was made between the productivity index for fractured and non-fractured rock and the results explained that the presence of fracture can improve the productivity index to about 5.74%.



**Figure 10.** Converting static geometry to dynamic geometry.

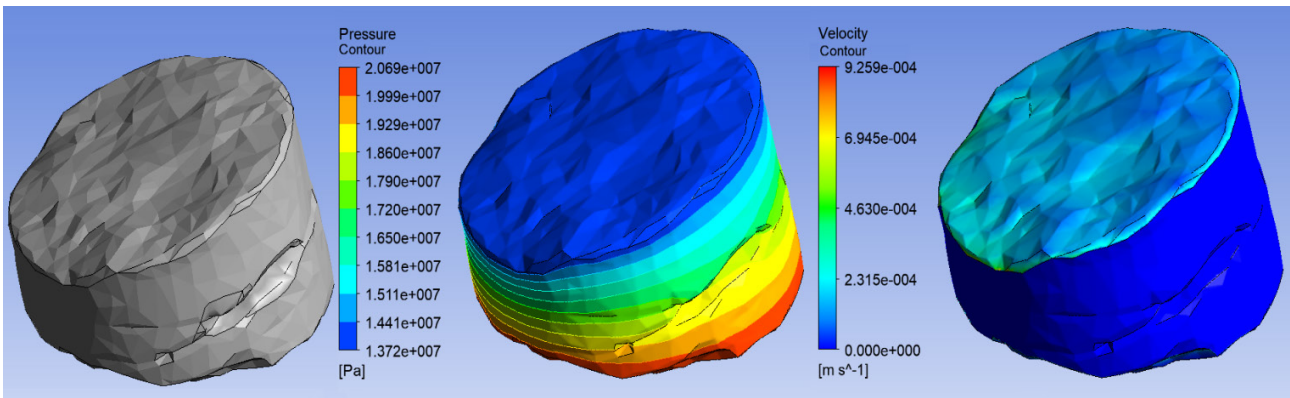


**Figure 11.** The pressure contour and velocity contour throughout the non-fractured rock

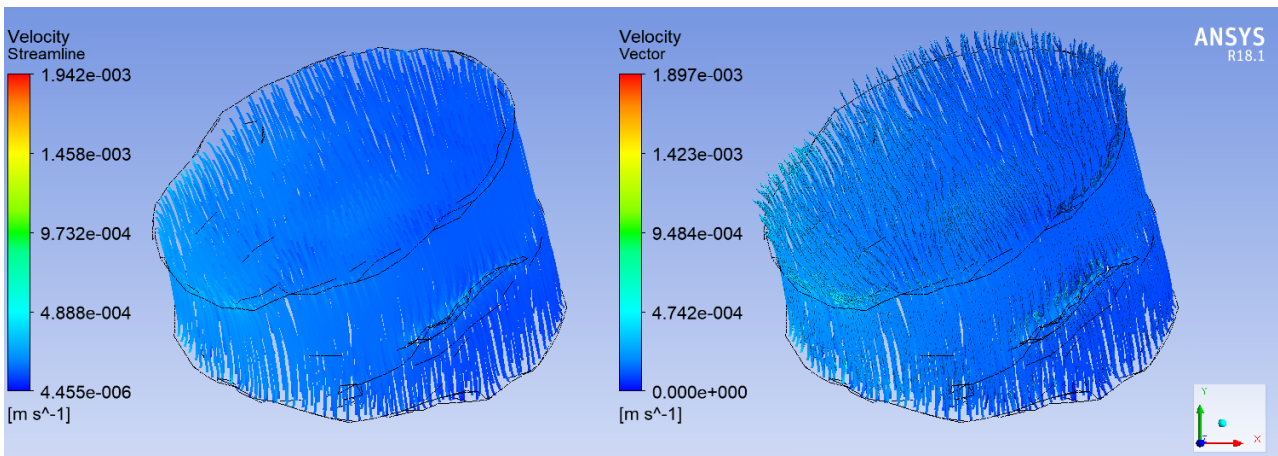


**Figure 12.** The velocity streamlines and the velocity vector throughout the non-fractured rock.

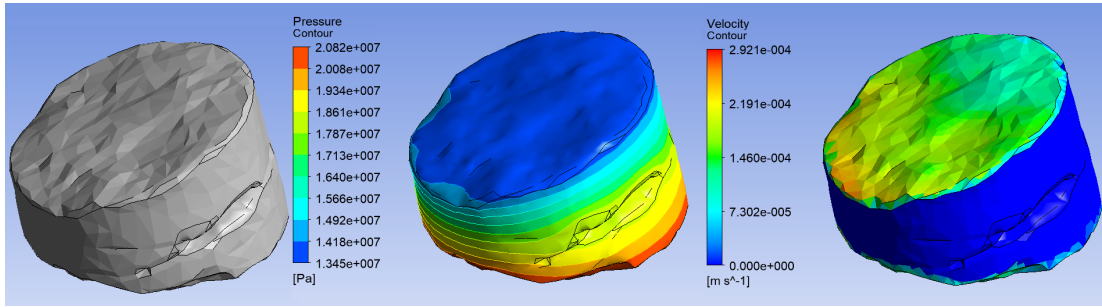


Figure 13. The pressure contour and velocity contour throughout the fractured rock.

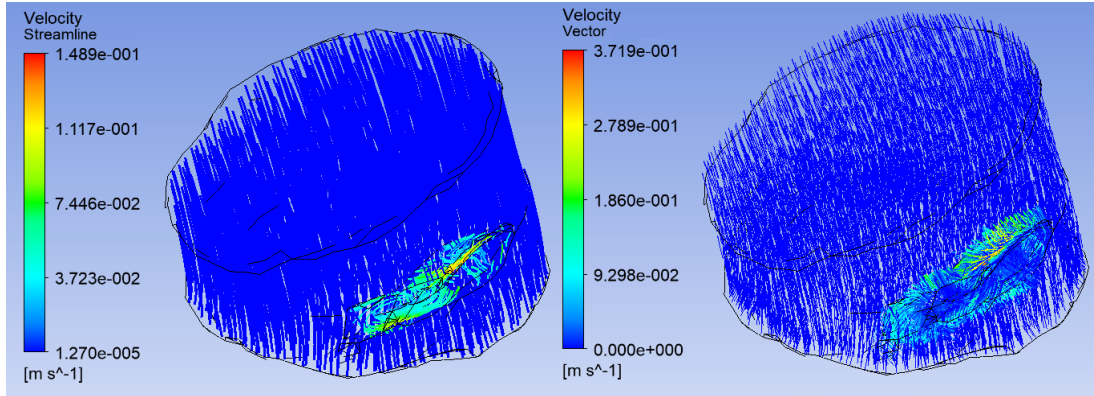
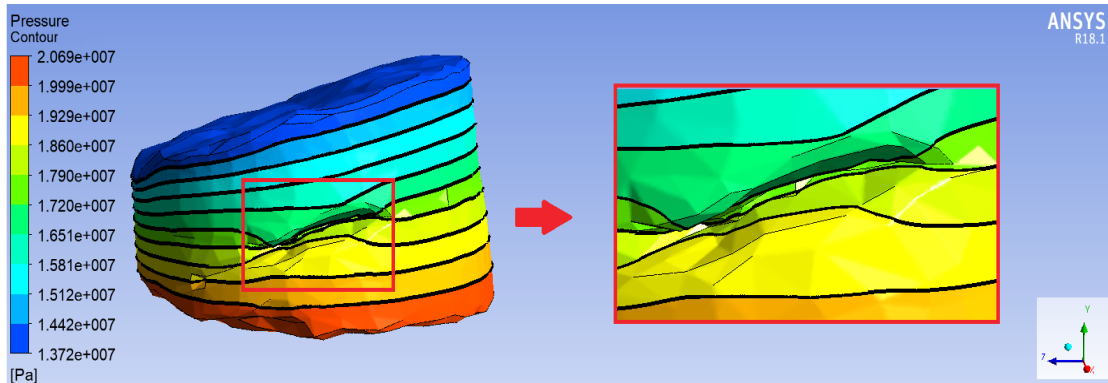
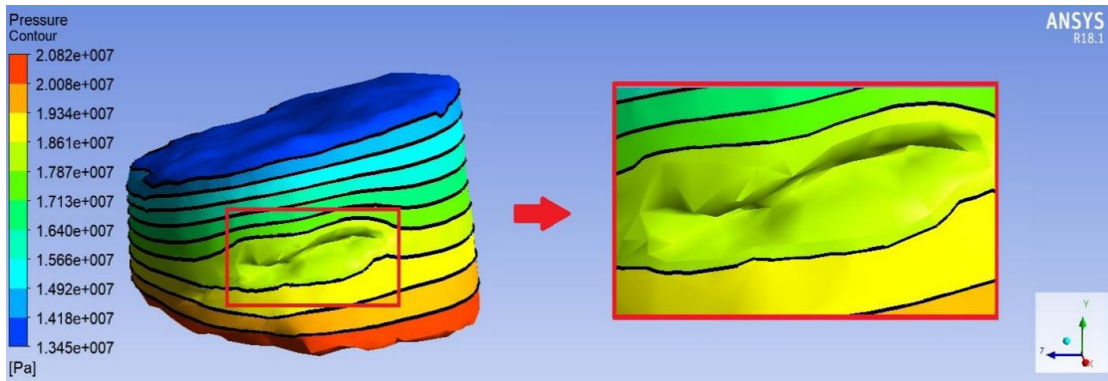


Figure 14. The velocity streamlines and the velocity vector throughout the fractured rock.



A) Non-Fractured Rock



B) Fractured Rock

Figure 15. The pressure contour of the rock.

#### 4. Conclusions

The numerical simulation for single-phase and laminar flow of fluid within fractured rock has been conducted in this study. The X-ray Computed Tomography (CT) imaging was successfully applied. However, the resulting images from the CT scan have been treated with several programs to get a three-dimensional dynamic domain. The three-dimension for fluid behavior in a rock has been illustrated. Moreover, the X-ray Computed Tomography (CT) imaging helped to diagnosis the fracture within the rock with high resolution and the behavior of fluid within the fracture has been visualized in detail. The results of this study explained that the presence of fracture can improve the productivity index to about 5.74%.

#### References

- [1] Tsang, Y.W.: The effect of tortuosity on fluid flow through a single fracture. *Water Resour. Res.* 20, 1209-1215 (1984).
- [2] Poon, C.Y., Sayles, R.S., Jones, T.A.: Surface measurement and fractal characterization of naturally fractured rocks. *J. Phys. D. Appl. Phys.* 25, 1269-1275 (1992).
- [3] Al-Yaarubi, A.H., Pain, C.C., Grattoni, C.A., Zimmerman, R.W.: Navier-Stokes simulations of fluid flow through a rock fracture. In: Faybishenko, B., Gale, J. (eds.) *Dynamics of fluids and transport in fractured rocks*, vol. 162 of AGU Monograph, pp. 55-64. American Geophysical Union, Washington, DC (2005).
- [4] Randolph, L., Johnson, B.: Influence of faults of moderate displacement on groundwater flow in the Hickory Sandstone aquifer in central Texas. *Abstracts - Geological Society of America* 21, 242 (1989).
- [5] Mozley, P.S., Goodwin, K.B.: Patterns of cementation along a Cenozoic normal fault: a record of paleo flow orientations. *Geology* 23, 539 - 542 (1995).
- [6] Barenblatt G., Zheltov I., and Kochina I., "Basic concepts in the theory of seepage of homogeneous liquids in fissured rocks [strata]", *Journal of applied mathematics and mechanics*, Vol. 24, No. 5, pp 1286-1303, 1960.
- [7] Odeh A. S., "Unsteady state behavior of naturally fractured reservoir", *Society of Petroleum Engineers Journal*, Vol. 5, No. 1, pp 60-66, March, 1965.
- [8] Kazemi H., "Pressure Transient Analysis of Naturally Fractured Reservoirs with Uniform Fracture Distribution", *Society of Petroleum Engineers Journal*, Vol. 9, No. 04, pp 451-462, 1969.
- [9] Pickett G. R., and Reynolds E. B., "Evaluation of fractured reservoir", *Society of Petroleum Engineers Journal*, Vol. 9, No. 1, pp 28-38, March 1969.
- [10] Abbasi M., Madani M., Shari M., and Kazemi A., "Fluid flow in fractured reservoirs: Exact analytical solution for transient dual porosity model with variable rock matrix block size", *Journal of Petroleum Science and Engineering*, Vol. 164, pp 571-583, 2018.
- [11] Al-Husseini A. J., Abood F. A., Alshara A. K., *Hydrodynamics Behaviour of Single and Multi Fracture with Different Orientations in Petroleum Reservoir*, *Basrah Journal for Engineering Sciences*, Vol.19, No.1, pp.12-16, (2019).
- [12] Majeed A. J., Alshara A. K., Al-Mukhtar A. M., Abood F. A.: *Fracturing Parameters in Petroleum Reservoirs and Simulation*. *Advances in Material Sciences and Engineering*. Pp. 491-8, (2020).
- [13] Luthi S. M. and Souhaitet P.: Fracture apertures from electrical borehole scans, *Geophysics*, Vol. 55, No. 7. pp 821-833, July, (1990).
- [14] Hirono, T., Takahashi, M., Nakashima, S.: In situ visualization of fluid flow image within deformed rock by X-ray CT. *Eng. Geol.* 70, 37-46 (2003).
- [15] Karpyn, Z.T., Grader, A.S., Halleck, P.M.: Visualization of fluid occupancy in a rough fracture using micro-tomography. *J. Colloid Interface Sci.* 307, 181-187 (2007).
- [16] Berg, R. R., "Method for determining permeability from reservoir rock properties". *Transactions Gulf Coast Association of Geological Societies*, Vol. 20, pp 303-317, (1970).
- [17] Guo B., Tao Y., Bandilla K., and Celia M., "Vertically Integrated Dual-porosity and Dual-permeability Models for CO2 Sequestration in Fractured Geological Formation", *Energy Procedia*, Vol. 114, pp 3343-3352, Nov., (2017).
- [18] Weirong L., Dong Z., and Lei G., "Integrating Embedded Discrete Fracture and Dual Porosity Method to Simulate Fluid Flow in Shale Oil Reservoir", *Energies*, Vol. 10, No. 10, (2017).
- [19] Hamdan M. H., "Single-Phase through Porous Channels A Review of Flow Models and Channel Entry Conditions". *Applied Mathematics and Computation* Vol. 62, No. 3, pp 203-222, May, 1994.
- [20] Rudraiah N., Chandrasekhara B. C., Veerabhadraiah R., and Nagaraj S. T., "Some Flow Problems in Porous Media", *PGSAM-2*, Bangalore University, India, 1979.

## NOMENCLATURE

Permeability [Darcy]	$k$
The phase saturation	$s$
Average reservoir pressure [psi]	$\bar{P}_R$
Bottom hole pressure [psi]	$P_{wf}$
Pressure gradient [psi]	$\nabla P$
Relative permeability	$k_r$
Gravity acceleration vector [ $m/s^2$ ]	$g$
Phase flux [m/s]	$u$
Volumetric flux from the matrix domain to the fracture domain [m/s]	$q^{m-f}$
Volumetric flux from the fracture domain to the matrix domain [m/s]	$q^{f-m}$
Velocity [m/s]	$v$
Time [s]	$t$
Productivity index [BBl/psi Day]	$J$
Oil flow rate [BBl/Day]	$q_o$
Greek Letters	
Volumetric source term [m/s]	$\psi$
Porosity [-]	$\phi$
The density of fluid [ $kg/m^3$ ]	$\rho$
Dynamic viscosity [Pa. s]	$\mu$
Superscripts	
Fracture	$f$
Matrix	$m$